Growth of Single-Walled Carbon Nanotubes from Discrete Catalytic Nanoparticles of Various Sizes

Yiming Li, Woong Kim, Yuegang Zhang, Marco Rolandi, Dunwei Wang, and Hongjie Dai*

Department of Chemistry, Stanford University, Stanford, California 94305

Received: May 31, 2001; In Final Form: August 29, 2001

Discrete catalytic nanoparticles with diameters in the range of 1−2 nm and 3−5 nm respectively are obtained by placing controllable numbers of metal atoms into the cores of apoferritin, and used for growth of single-walled carbon nanotube (SWNTs) on substrates by chemical vapor deposition (CVD). Atomic force microscopy (AFM), transmission electron microscopy (TEM), and micro-Raman spectroscopy are used to characterize isolated nanotubes grown from the discrete nanoparticles. The characterizations, carried out at single-tube and single-particle level, obtain clear evidence that the diameters of nanotubes are determined by the diameters of catalytic nanoparticles. With nanoparticles placed on ultrathin alumina membranes, isolated SWNTs are grown and directly examined by transmission electron microscopy. For the first time, both ends of an as-grown single-walled nanotube are imaged by TEM, leading to a microscopic picture of nanotube growth mechanism. It is shown that controlling the structures of catalytic nanoparticles allows the control of nanotube diameter, and could also enable the control of SWNT length and eventually chirality.

Introduction

Single-walled carbon nanotubes are molecular scale wires with interesting and potentially useful properties.[1] It is well-established that the diameter and chirality of a SWNT determine the electronic structures of the nanotube.[1] Therefore, to obtain homogeneous nanotube materials with specific physical properties, it is necessary to control the structures of nanotubes by chemical synthesis methods. The prerequisite for such control is a detailed understanding of the growth mechanism of nanotubes.

It has been shown that chemical vapor deposition on catalytically patterned surfaces offers unique advantages in the growth of self-organized nanotubes at specific locations with desired orientations.[2,3] However, typical catalyst materials used for SWNT growth consist of metal oxide nanoparticles formed on high surface-area support powders by impregnation methods or by using mixed liquid-phase catalyst precursors.[4−11] The structures (e.g., sizes) of the catalytic nanoparticles are not well characterized or controlled, as the nanoparticles are largely buried in the powdery support material. As a result, the produced SWNTs typically exhibit a large diameter distribution (from 1 nm up to 5 nm).[6] Clearly, a much better control of the catalytic nanoparticles is needed in order to control the structures of SWNTs by CVD growth approaches. Furthermore, it is necessary to learn about the roles played by nanoparticles in producing nanotubes and in determining the nanotube structures.

TEM has been a powerful technique to characterize nanotubes synthesized by various methods. In particular, by imaging the ends of nanotubes with TEM, one can glean their growth mechanism.[6,12] For CVD growth of SWNTs using methane as carbon feedstock, it has been suggested that SWNTs grow via the base-growth mode with the catalytic nanoparticle 'seeds' remaining anchored on the support during growth.[4−6,13,14] It is also suggested that the size of the catalytic nanoparticle determines the diameter of the SWNT. Nevertheless, with supported powdery catalyst materials, the particle-containing ends of SWNTs are always buried in the support and therefore impossible to image in TEM. Thus far, microscopy data clearly revealing particle-tube relationships has been lacking to prove the aforementioned suggestions about SWNT growth.

Recently, Liu and co-workers synthesized isolated Fe nanoparticles and used them for CVD growth of SWNTs.[13,14] The nanoparticles were formed in reverse-micelles in organic solutions and the particle sizes were controllable from 3.6 to 14 nm within 10% dispersion. Nevertheless, a relationship between the particle size and the nanotube diameter was not established. It remains to be shown that by purposely varying the size of the nanoparticles, one can control the diameter of SWNTs systematically by CVD growth. Also, it is desirable to obtain discrete particles with diameters in the range of 1−2 nm.

Here, we report the synthesis of discrete catalytic iron oxide nanoparticles with tunable diameters by making use of an iron-storage protein, ferritin.[15] We are able to grow isolated single-walled carbon nanotubes from the discrete nanoparticles by CVD, and demonstrate that the diameters of SWNTs can be controlled by varying the sizes of catalytic particles. The ferritin protein consists of a 12 nm diameter spherical shell made of 24 polypeptide subunits. The central core of ferritin is approximately 8 nm in diameter, and can store up to 4 500 iron atoms in the form of hydrous ferric oxide. It has been shown previously that the core of ferritin can be emptied to afford apoferritin, and subsequently, a controllable number of Fe (III) atoms can be put back into the core.[16−20] This method has proven useful in synthesizing nanometer-sized nanoparticles with narrow size distributions. Here, using a slightly modified method, we place ∼200 Fe(III) into the cores of apoferritins in aqueous solutions to obtain artificial ferritin (termed 's-ferritin') (Scheme 1). The synthesized ferritins are automatically stabilized against agglomeration in aqueous solutions by functional groups on the proteins, and allow the deposition of isolated ferritin on various substrates. Upon high temperature calcination to remove the organic shells and fully oxidize the iron core, discrete iron oxide nanoparticles with mean diameter 1.9 nm are obtained

10.1021/jp012085b CCC: $20.00
Published on Web 10/31/2001

SCHEME 1. Process Flow for SWNT Synthesis from Discrete Nanoparticles by CVD

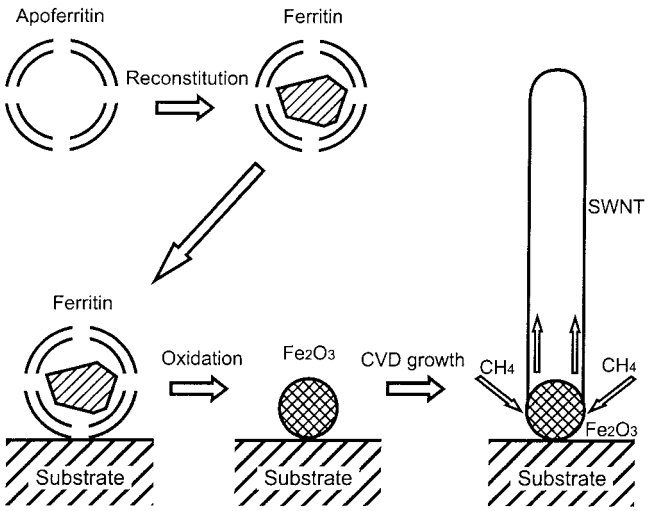

on the substrate. CVD growth with the substrate produces SWNTs from the discrete catalytic nanoparticles (Scheme 1), and the average diameter of the nanotubes (~1.5 nm) is found to be close to that of the nanoparticles. To vary the size of iron oxide nanoparticles, we place ~1100 Fe(III) in the cores of apoferritin (termed 'm-ferritin'). Catalytic nanoparticles derived from the m-ferritin are ~3.7 nm in diameter, and the mean diameter of the produced SWNTs is ~3.1 nm.

An important development by the current work is the ability to characterize isolated as-grown SWNTs by transmission electron microscopy. We place discrete catalytic nanoparticles on ultrathin alumina membranes formed directly on TEM grids, and grow SWNTs from the nanoparticles by CVD. Because the alumina membranes are transparent to electron beams, we are able to image both the nanoparticles and the nanotubes without any treatment (e.g., nanotube dispersion in solvents by sonication, deposition on grids) to the sample typically involved in TEM studies of nanotubes. For the first time, we observe both ends of CVD-grown SWNTs in the TEM, which allows us to learn about the microscopic particle-tube relationship and the growth mechanism of nanotubes. The understanding thus obtained should be useful for controlling nanotube diameter, length, and eventually chirality.

Finally, we have carried out surface enhance resonance Raman studies of isolated SWNTs grown from nanoparticles on SiO_2. The spectroscopic measurements confirm the high quality of the nanotubes and obtain additional information about the structures of the synthesized nanotubes.

Experimental Section

Materials. Horse spleen apoferritin, 2-(N−Morpholino)-ethanesulfonic acid (MES) buffer, ammonium iron (II) sulfate, trimethylamine-*N*-oxide (Me_3NO) and aluminum chloride were purchased from Sigma-Aldrich and used as received. Regenerated cellulose dialysis membranes were purchased from Spectra/Pro with a molecular weight cutoff of 12 000−14 000. Gold microgrids for TEM were obtained from Ted Pella Inc. Triblock copolymer P123 involved in making porous alumina membrane was obtained from BASF.

Synthesis of Artificial Ferritin by Fe Loading into Apoferritin. A 10 mg (0.022 μmol) portion of apoferritin from horse spleen was added to 50 mL MES buffer solution (0.05 M, pH adjusted to 7.0 by NaOH). The solution was heated to 50 °C and constantly stirred. 35 μL of 0.025 M ammonium iron (II) sulfate (corresponding to 40 Fe/apoferritin loading) was added dropwise to the apoferritin solution, followed by addition of Me_3NO (0.025 M, 35 μL) to fully oxidize Fe(II) to Fe(III). This procedure was repeated 5 times at 15 min intervals to achieve a theoretical loading of ~200 Fe(III)/ferritin. The resultant solution was dialyzed overnight against distilled water at 4 °C, and then centrifuged at 16 000 g for 15 min in order to remove any potential aggregates. The final solution contained 0.44 μM of the synthesized s-ferritin in pure water. The solution was stored at 4 °C when not in use. The synthesis of m-ferritin followed the same procedure as above except for higher (1100) Fe loading into apoferritin.

Deposition of Ferritin on Substrates and Formation of Fe_2O_3 Nanoparticles. The synthesized artificial ferritin solutions were used to deposit isolated ferritin onto SiO_2 substrates. Deposition was done by incubating silicon chips with 500 nm thick thermally grown surface-oxide in the ferritin solutions at 4 °C overnight. The substrates were rinsed with deionized water and then blow-dried. To obtain iron oxide nanoparticles, the substrates were heated to 800 °C in air and calcined for 5 min to remove the organic shell of the deposited ferritin. This led to the formation of discrete Fe_2O_3 nanoparticles on the SiO_2 substrates. The Fe_2O_3 nanoparticles thus formed were characterized by an atomic force microscope (AFM) operated in the tapping mode with commercial silicon cantilevers (spring constant 1 N/m) with integrated tips.

Synthesis of Single-Walled Carbon Nanotubes. Synthesis of SWNTs from discrete Fe_2O_3 nanoparticles formed on substrates was performed by using a CVD approach described previously.[8] In brief, the substrates were placed into the center of a 1" quartz tube reactor and heated to 900 °C in a tube-furnace. Methane (200 sccm, 99%) and hydrogen (200 sccm) were passed through the tube reactor for 5 min, followed by cooling the CVD system in Ar to room temperature. Note that we made a slight modification here to the gas flow rate from previous conditions (methane at 1000 sccm), as we found that low flow-rate of methane accompanied by a hydrogen co-flow could prevent any pyrolysis problem.[21]

TEM of Ferritin. We used TEM to image the iron cores of the synthesized ferritin. TEM sample preparation was done by first wetting a holey-carbon TEM grid by methanol, and then placing a drop of the ferritin solution onto the grid. The methanol pre-wetting step allowed the dispersion of discrete ferritin molecules on the holey-carbon film needed for TEM imaging. Without this step, few ferritins were found to deposit due to the highly hydrophobic nature of the carbon film.

Growth of SWNTs on Ultrathin Al_2O_3 Membranes and TEM Imaging of As-Grown Nanotubes. A key step for imaging as-grown SWNTs by TEM was to form ultrathin mesoporous alumina membranes on gold microgrids, done by dipping commercially available gold microgrids into a mixed ethanol and butanol solution of a P123 triblock copolymer (2.8 mM) and aluminum chloride (0.16 M). The grids were then calcined at 500 °C for 12 h in air to remove the polymer component, leaving a mesoporous alumina[22] membrane (several nanometers thick) over the microgrids. A drop of the s-ferritin solution was applied to the grid and slowly dried in air to obtain dispersed ferritin on the alumina membrane. The grids were calcined at 800 °C for 5 min to form discrete Fe_2O_3 nanoparticles and used for CVD growth of SWNTs. After the growth, the microgrids were directly mounted onto a Philips CM20 TEM to image the SWNTs and investigate their relationships with catalytic nanoparticles. This approach allowed TEM study of

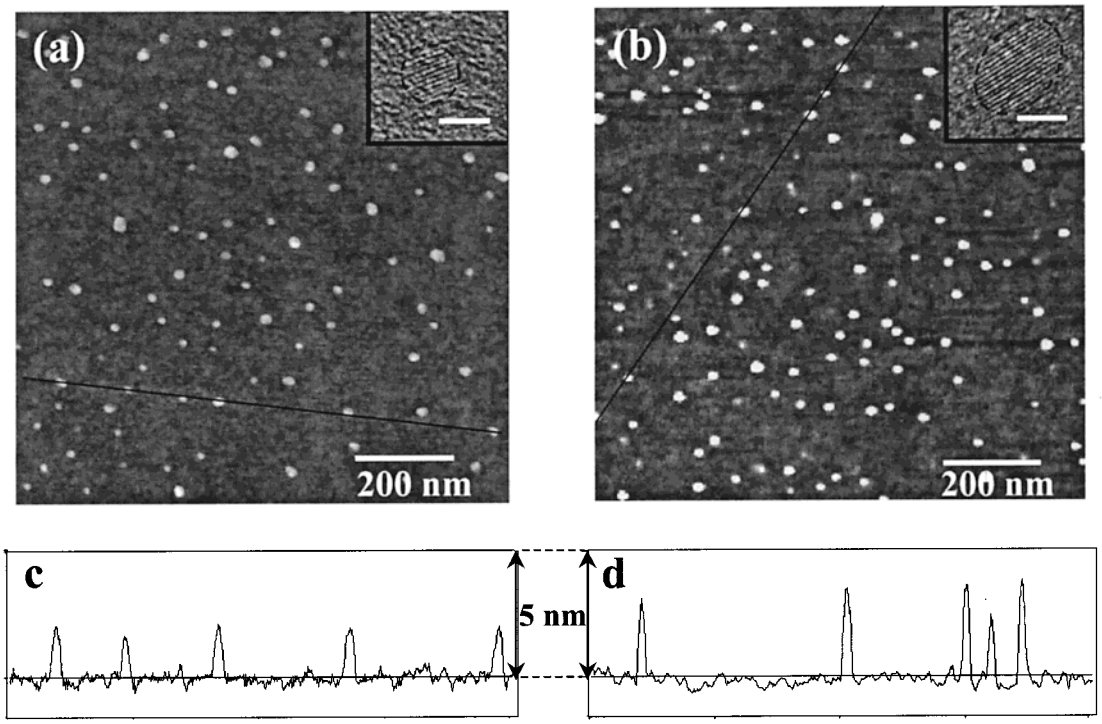

Figure 1. (a) AFM topography image of discrete Fe_2O_3 nanoparticles (bright dots) derived by calcination of s-ferritin deposited on SiO_2. Inset: A high magnification TEM image of the Fe core of an s-ferritin before calcination (scale bar: 3 nm). The dashed circle is drawn to enclose and highlight the core, as the contrast between the core and the carbon film is not high due to the small core-size. (b) An AFM topography image of Fe_2O_3 nanoparticles derived by calcination of m-ferritin deposited on SiO_2. Inset: A high magnification TEM image of the Fe core of an m-ferritin before calcination (scale bar: 3 nm). The z-ranges for image (a) and (b) are the same, 8 nm. (c) and (d) are the topographic height measurements for nanoparticles along the line-cuts (black lines) in (a) and (b), respectively.

SWNTs and catalytic nanoparticles without any sample processing after nanotube growth.

Micro-Raman Characterization of Isolated SWNTs Grown on SiO_2. A Renishaw 1000 micro-Raman system was used to record Raman spectra of SWNTs grown from discrete catalytic nanoparticles formed on SiO_2 substrates. The excitation wavelength was 788 nm (1.58 eV) sourced by an AlGaAs diode laser. A 50× objective was used to focus the laser beam down to a ~1 μm diameter spot on the sample. The scattered light was collected by the same objective, passed through a notch filter to minimize Raleigh scattered components before detection.

Our samples contained isolated SWNTs distributed on the substrate. Only a limited number (0−5) of SWNTs were under the focused 1 μm diameter laser spot. For micro-Raman experiments, we coated the samples with 35 Å of Au by electron beam evaporation to form gold nanoclusters with average diameter ~5 nm on the SWNTs as found by AFM. Similar clustering of Au was observed on suspended SWNTs previously.[23] The Au decoration of SWNTs allowed the detection of phonon modes of a small number of isolated SWNTs via surface enhanced resonance Raman effect.[24]

Results and Discussion

Formation of Catalytic Nanoparticles. TEM imaging clearly revealed the iron containing cores of the synthesized ferritin (insets of Figure 1). Iron incorporation into the apoferritin core is known to be a multistep process involving the binding and migration of Fe(II) to the ferroxidase site, Fe(II) oxidation, Fe(III) hydrolysis and nucleation and growth of the mineral core.[19] The average diameter of the iron core is approximately 3 nm for the s-ferritin, and 5 nm for the m-ferritin before calcination. After deposition on a SiO_2 substrate and calcination in air at 800 °C for 5 min, the organic shell of ferritin were removed, leaving dispersed iron oxide nanoparticles on the surface. Figure 1, parts a and b, shows AFM images of discrete iron oxide nanoparticles derived from s-ferritin and m-ferritin, respectively. Because the apparent widths of the nanoparticles in the AFM data do not reflect the true particle sizes due to AFM tip (radius 10−15 nm) convolution, we measured the

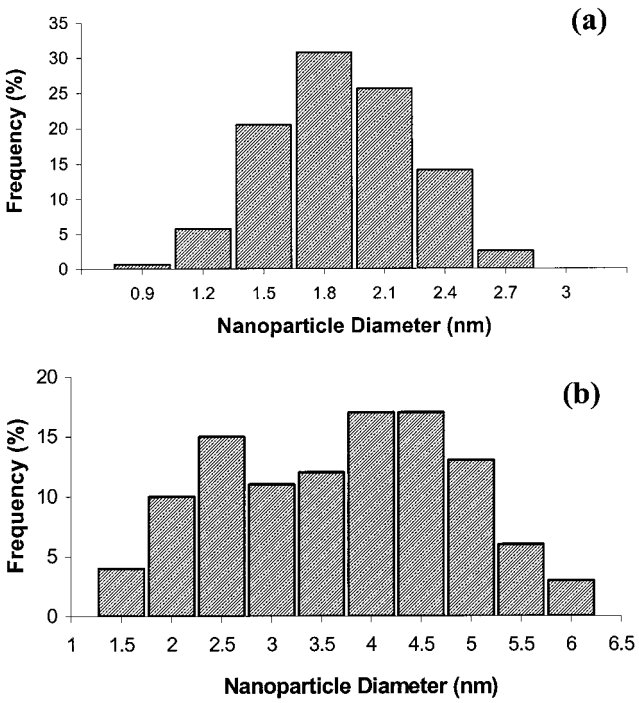

Figure 2. (a) Diameter distribution for Fe_2O_3 nanoparticles derived from s-ferritin. (b) Diameter distribution for Fe_2O_3 nanoparticles derived from m-ferritin.

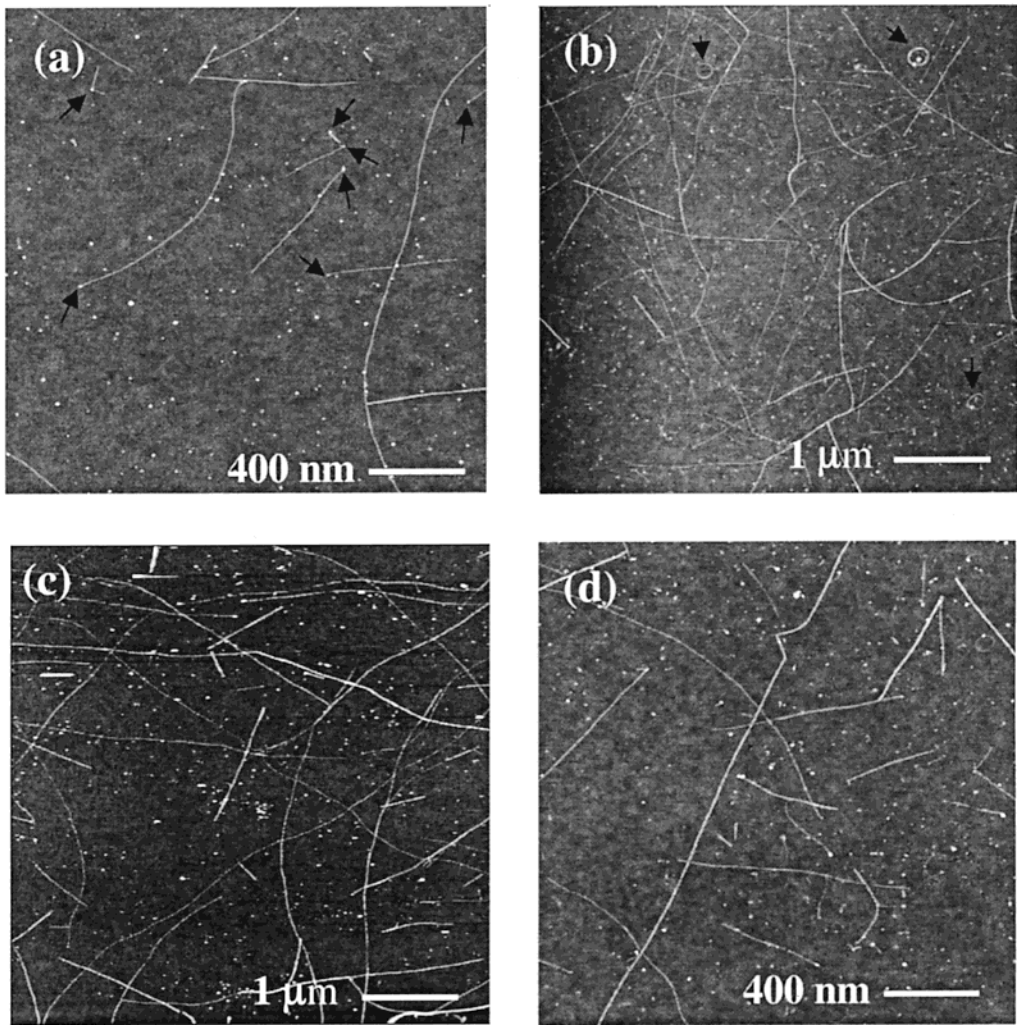

Figure 3. (a)−(d) AFM topography images of nanotubes grown from catalytic nanoparticles derived from s-ferritin deposited on SiO_2. The arrows in (a) point to the ends of nanotubes that appear attached to nanoparticles. The arrows in (b) point to several circular tube structures.

particle diameters from their topographic heights (Figure 1c and 1d).

The size distribution of nanoparticles derived from s-ferritin is shown in Figure 2a. The result was obtained by measuring 154 nanoparticles and showed that the diameters of the nanoparticles were $\sim 1.9 \pm 0.3$ nm. On the basis of the crystal structure or mass density of Fe_2O_3 and assuming the nanoparticles were roughly spherical, we estimated the average number of iron atoms in the nanoparticles to be ~150, close to the theoretical 200 Fe/ferritin loading for the s-ferritin. We also performed AFM imaging of the same surface regions on the ferritin-dispersed substrates before and after calcination. The deposition step always led to discrete ferritin particles on the substrate, and every ferritin yielded one nanoparticle with a reduction in the apparent height after the removal of the organic-shell. Diameters of nanoparticles derived from m-ferritin were $\sim 3.7 \pm 1.1$ nm (Figure 2b), larger than those derived from the s-ferritin, as a result of higher iron loading (Figure 1c vs 1d).

AFM of Nanotubes Grown from Discrete Nanoparticles on SiO_2. Figure 3 shows AFM images of nanotubes grown from nanoparticles derived from s-ferritin dispersed on SiO_2 substrates. Most of the nanotubes have lengths in the range of $\sim 0.5-5$ μm, whereas the longest nanotubes were ~ 20 μm and the shortest tubes were only tens of nanometers in lengths. The diameters of the nanotubes were measured by their apparent heights from AFM topography data. Measurements carried out with 93 nanotubes found that the nanotube diameters were 1.5 ± 0.4 nm (see histogram shown in Figure 5a), close to the diameter distribution of the nanoparticles (1.9 ± 0.3 nm) shown in Figure 2a.

From the AFM data, most of the SWNTs appeared to have an identifiable nanoparticle attached at one end (Figure 3a). However, with AFM, it is not possible to resolve the nanoparticles unambiguously and establish a clear particle-tube relationship. These issues will be addressed by TEM imaging of as-grown nanotubes on thin alumina membranes in a later section.

Most of the nanotubes grown from discrete nanoparticles deposited on SiO_2 appeared straight, and some of them are curved smoothly along their lengths. The curvatures are attributed to the flexibility of nanotubes due to their high aspect ratios. Occasionally, we observed nanotubes with kinks along their lengths (Figure 3d), but the occurrence of such kinks is rare. It is possible that the kinks are formed due to mechanical forces exerted on the nanotubes as the tubes land on the substrate during growth. However, we cannot rule out the possibility of kink formation by topological defects in the nanotube structure. Unexpectedly, we have also encountered rare occurrences of nanotubes forming circular loops (Figure 3b) resembling the 'crop circles' previously sighted in SWNT materials grown by laser ablation.[25] The nanotube loops in our samples have diameters ~200 nm. It was reported earlier that bubble formation

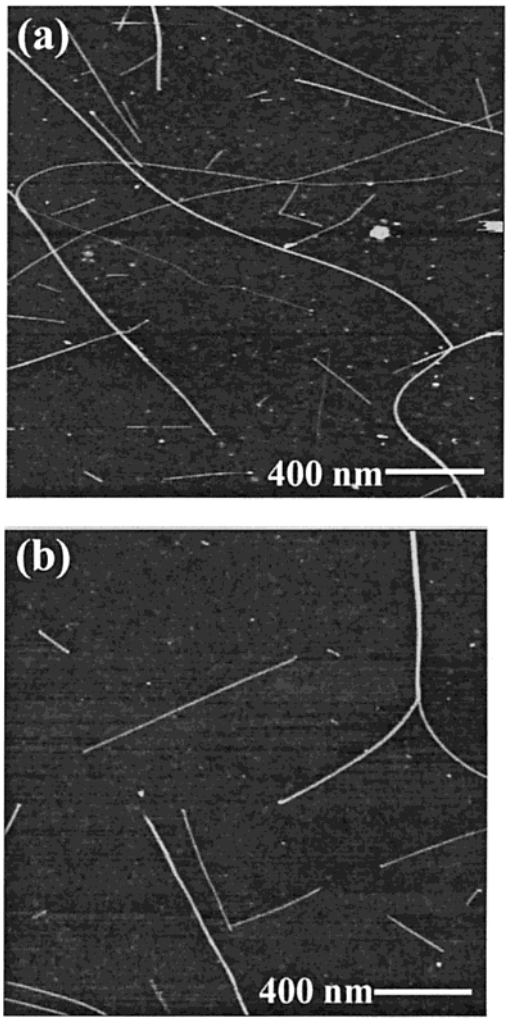

Figure 4. (a)−(b) AFM topography images of nanotubes grown from catalytic nanoparticles derived from m-ferritin deposited on SiO_2.

during sonication of SWNTs suspended in a solvent could lead to the formation of circular loops of SWNTs.[26] In our case, the nanotube loops were undoubtedly formed in the growth stage because the nanotubes received no sonication or any other treatment after their growth. The most plausible cause for their formation is the annihilation of two ends of a nanotube during growth,[25] and the circular shape of the loop should be due to structural bending/deformation of the nanotube.[25]

The nanotubes grown from dispersed catalytic nanoparticles were largely isolated, in the sense that bundling of nanotubes grown from different particles only occurred in areas where the nanotube density was high, and therefore, the likelihood of nanotubes binding together via van der Waals force was high. It was observed that not every nanoparticle dispersed on the substrate produced a nanotube, as the number of tube-like structures is small compared to the number of nanoparticles in a given area (dots in Figure 3).

AFM images of nanotubes grown from nanoparticles derived from m-ferritin are shown in Figure 4. The histogram plot in Figure 5b, obtained by measuring about 100 tubes, shows that the diameters of the nanotubes are 3.0 ± 0.9 nm, close to the diameters of the nanoparticles (3.7 ± 1.1 nm, Figure 2b). Combined with data obtained with the s-ferritin (nanotubes diameter $\approx 1.5 \pm 0.4$ nm; nanoparticles diameter $\approx 1.9 \pm 0.3$ nm), these results show that the diameters of nanotubes are closely related to the diameters of catalytic nanoparticles.

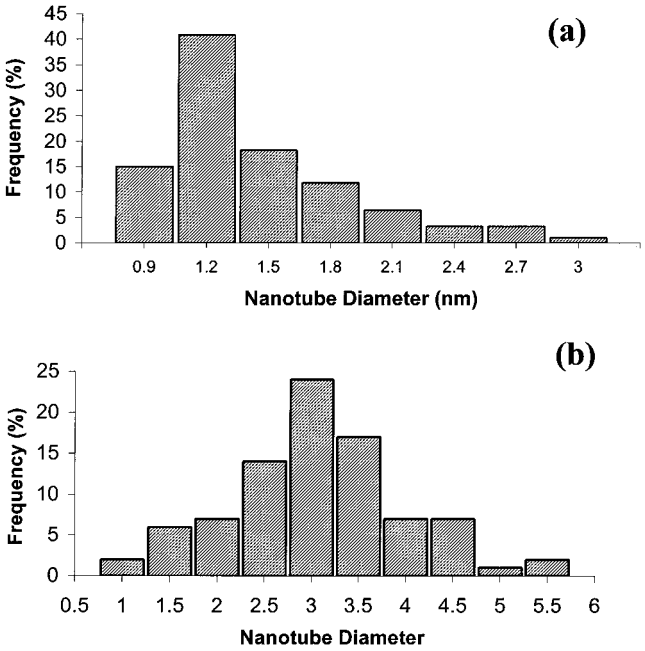

Figure 5. (a) Diameter distribution of nanotubes grown from nanoparticles derived from s-ferritin. (b) Diameter distribution of nanotubes grown from nanoparticles derived from m-ferritin.

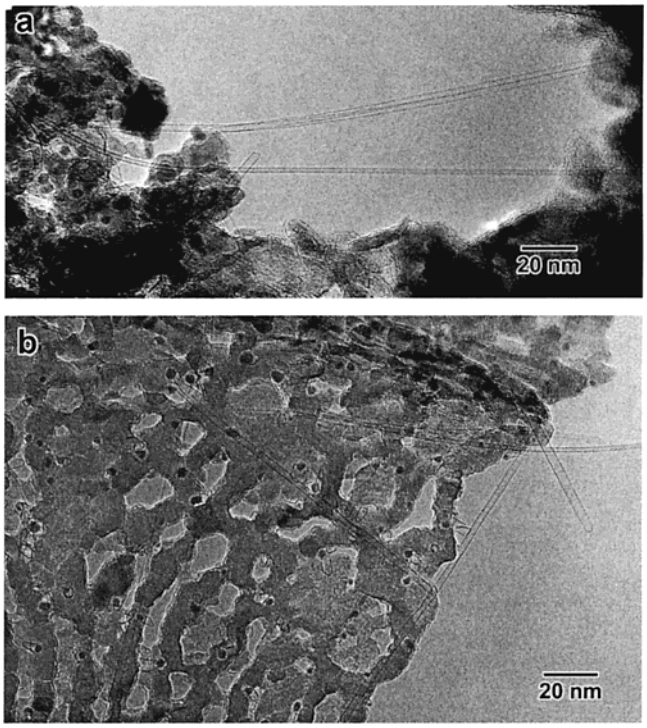

Figure 6. TEM images of SWNTs as grown on ultrathin alumina membranes formed directly on TEM micro-grids. (a) A TEM image showing the synthesized SWNTs. (b) A TEM image showing SWNTs and discrete nanoparticles (black dots) on the porous alumina membrane.

TEM of As-Grown SWNTs. We have characterized nanotubes grown from catalytic nanoparticles dispersed on thin alumina membranes by TEM. The data shown here are obtained with nanoparticles derived from s-ferritin. Figure 6 clearly shows that indeed, high quality SWNTs are synthesized from discrete catalytic nanoparticles dispersed on the membrane. The nanotubes are mostly individual SWNTs, although small bundles are occasionally observed (Figure 6a).

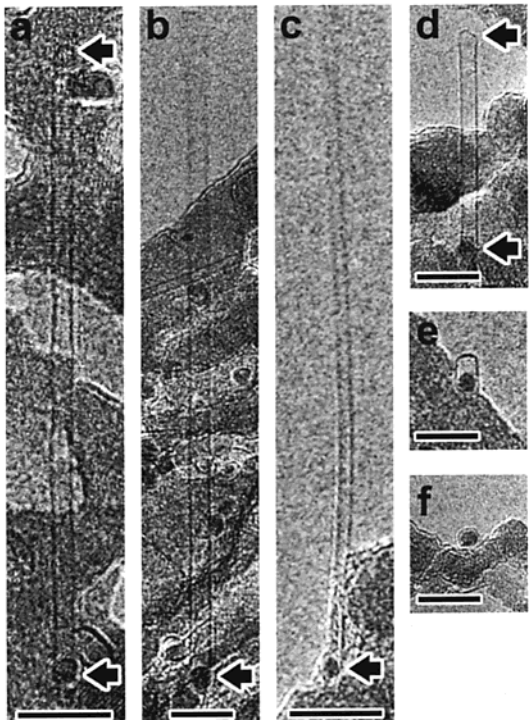

Figure 7. TEM images showing particle-nanotube relationships. (a)−(d), SWNTs grown from discrete nanoparticles (dark dots at the bottom of the images). The arrows point to the ends of the nanotubes. The ends extended out of the membrane in (b) and (c) could not be imaged due to thermal vibration. The background reflects the alumina membrane morphology. (e) Image of an ultra-short (∼4 nm) nanotube capsule grown from a ∼2 nm nanoparticle. (f) Image of a nanoparticle surrounded by a single graphitic-shell. Scale bars in (a)−(f): 10 nm.

Previously, typical catalysts for CVD growth of SWNTs are catalytic nanoparticles formed on high surface area support materials including silica and alumina powders.[4−10] TEM imaging of CVD grown SWNTs from such a catalyst could observe one of the nanotube ends, but the other end is typically buried or hidden in the powdery catalyst materials.[4−6] Here, we were able to image both ends of SWNTs grown from the discrete catalytic nanoparticles (Figure 7a, d, e). In Figure 7a, the 70 nm long SWNT has one of its ends containing a nanoparticle (bottom arrow) and the other end dome-closed (top arrow). The diameter of the nanotube is identical to that of the nanoparticle. Figure 7, parts b and c, shows two SWNTs with one end starting from a nanoparticle anchored on the alumina membrane and the other end extending out of the membrane. The end of the tube outside of the membrane is not clearly imaged due to thermal vibration of the unsupported SWNT segment. Figure 7d shows that the particle-containing end of a SWNT is on the alumina membrane, and the other end is closed and extended out of the membrane. Importantly, we have not seen a SWNT extending out of the membrane with the extended-end of the tube tipped by a catalyst nanoparticle.

TEM imaging found that only a fraction of the nanoparticles produced SWNTs with appreciable lengths. Some of the nanoparticles produced short nanotube 'capsules' with lengths on the order of tens of nanometers down to 4 nm (Figure 7e). These short tubes were not resolved by AFM imaging because the AFM tip radius is too large to resolve the capsule structures. Nanoparticles that produced no tubes showed a single graphitic shell surrounding the nanoparticles (Figure 7f). Note that prior to nanotube growth, our TEM study revealed no shell structures around the metal nanoparticles as the organic shells of ferritin were fully removed by calcination in air at 800 °C.

Nanotube Growth Mechanism. TEM imaging of both ends of isolated SWNTs lead to a microscopic picture of the nanotube growth mechanism in the CVD process. The results provide a clear evidence for the base-growth model[4−6,13,14,27−30] of SWNTs. That is, the catalyst nanoparticle remains on the supporting substrate, whereas a nanotube grows out from the particle with a closed-end (Scheme 1). This conclusion is based on TEM images that unambiguously show individual SWNTs with one end containing a catalyst nanoparticle and the other end closed. For SWNTs extending out of the support membrane, the extended-out ends are always closed, and particle-containing ends are observed on the membrane. We can therefore rule out the tip-growth model in which a SWNT grows with the catalytic particle lifting off from the substrate.

At the early stage of the CVD reaction, carbon atoms catalytically decomposed from methane are absorbed into the nanoparticle anchored on the support substrate, forming a carbon-iron solid-state solution in the particle. Once a super-saturation point is reached, carbon precipitates out from the particle surface. If carbon supply to the nanoparticle continues, continued carbon precipitation occurs and leads to the growth of a single-walled nanotube (Scheme 1). The growth terminates when the carbon supply to the nanoparticle becomes insufficient, leading to the formation of a nanotube with finite length. The precise cause of carbon supply shortage to a given nanoparticle during growth requires further elucidation. However, with a SWNT growing out from an anchored nanoparticle, it is not difficult to see that very limited surface area is available for the nanoparticle to uptake carbon from the gas phase. The nanoparticle is in intimate contact with the substrate and at the same time partially covered by the nanotube (Scheme 1), leaving a small surface area of the particle at the gas-nanoparticle interface. Catalyst poisoning effects could inactivate the interface and cut off the carbon supply to the particle. These poisoning effects may be due to amorphous carbon deposition on the nanoparticle, or undesired changes in particle-support interactions during growth. Further work is clearly required to address these possibilities.

There are significant disparities among nanoparticles in yielding SWNTs. As seen from AFM and TEM data, the nanoparticles produce SWNTs with a wide range of lengths (0.01−10 μm). Some particles appear inactive in producing nanotubes and yield only single spherical graphitic shells around the particles. One obvious disparity among the particles is the differences in size. Nanoparticles derived from the synthesized s-ferritin have a diameter distribution between approximately 1 and 3 nm. Comparing the nanotube and particle size distributions (Figure 2a vs Figure 5a), one can see that smaller nanoparticles ($<$ ∼1.8 nm) tend to be more active in producing SWNTs with appreciable lengths. A similar trend is found with SWNTs grown from nanoparticles derived from the m-ferritin. This could be attributed to that small particles allow carbon supersaturation readily and facilitate nanotube growth. We have also carried out preliminary growth studies using nanoparticles with diameters centered around ∼7 nm. However, no SWNTs are produced by these large particles, which supports the suggestion that large ($>$ 5−6 nm) nanoparticles are less active in producing SWNTs and is consistent with the finding by Liu.[14]

The differences in particle size cannot fully account for the different lengths of SWNTs (0 to 10 μm) grown from the particles. Our TEM study observed that even for nanoparticles with similar size, only a fraction of them produced SWNTs with appreciable length ($>$0.1 μm). A detailed understanding of this phenomenon is not yet at hand. We propose that inhomogeneity

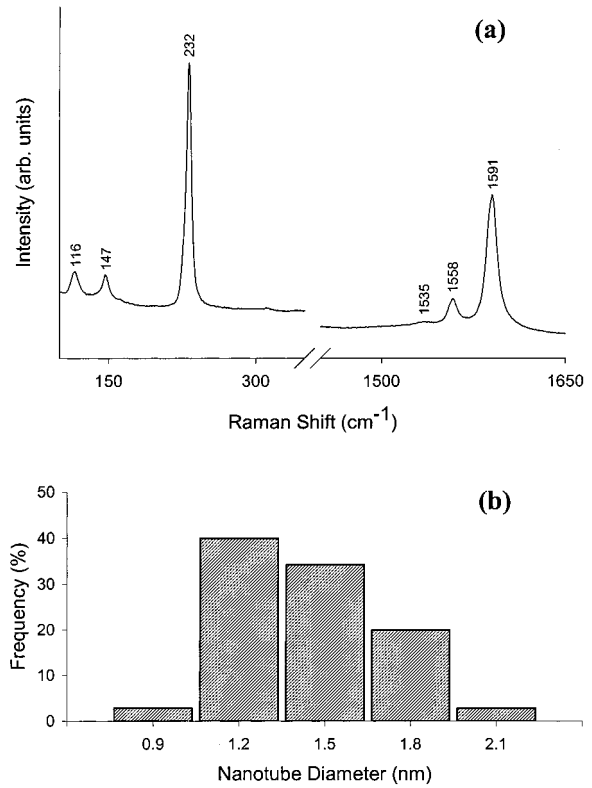

Figure 8. (a) Representative micro-Raman spectrum of several SWNTs grown from nanoparticles derived from s-ferritin. (b) Nanotube diameter distribution sampled by resonance micro-Raman measurements.

of the support substrate and variations in particle-support interactions over the support surface are responsible for the different activities of nanoparticles in producing nanotubes. The nature of the interactions and the detailed particle-substrate local binding configuration could be critical to the catalytic activity of the particle. These factors could determine how a nanoparticle uptake carbon from the gas phase, and how carbon saturate and precipitate from the nanoparticle. For instance, the gradient of carbon concentration in the nanoparticle should determine the direction of carbon precipitation from the particle,[27−29] whereas the carbon concentration in the nanoparticle must depend on the detailed particle-substrate geometry. Careful TEM examinations have found that some SWNTs appear to have grown parallel to the plane of the alumina membrane (Figure 7a), and some appear to have grown out from the particle at an angle with respect to the substrate plane, and land on the substrate when the tube reaches certain lengths. These observations support the suggestion that particle-support configurations may vary from particle to particle. One of the causes for such differences could be random surface roughness which is up to ~0.5 nm for SiO_2 and larger for alumina substrates.

Micro-Raman Characterization. We have used surface enhanced resonant Raman spectroscopy (SERRS)[24] to characterize small numbers of isolated SWNTs in ~1 μm^2 areas on SiO_2. SWNTs show characteristic low energy peaks in their Raman spectra corresponding to the radial breathing vibrational modes with A_{1g} symmetry.[31] The Raman shift (ω_{RBM}, in cm^{-1}) of this vibrational mode for an individual SWNT is related to its diameter (d, in nm) by $d = 248\ cm^{-1}\ nm/\omega_{RBM}$.[32] An estimate of the nanotube diameter distribution can be made from spectroscopic measurements.

Figure 8a shows a typical micro-SERRS spectrum acquired with several SWNTs grown from nanoparticles derived from s-ferritin on a SiO_2 substrate. The three peaks at 116, 147, and 232 cm^{-1} are identified as the radial breathing modes of three SWNTs with diameters of 2.1, 1.7, and 1.1 nm respectively. Three peaks at 1535, 1558, and 1591 cm^{-1} are observed at higher Raman shifts than the radial breathing modes. These peaks correspond to the splitting of in-plane vibrational modes of a graphene sheet centered at 1580 cm^{-1}, as a result of symmetry lowering from graphene to nanotubes. The separation between the split peaks is also diameter dependent, and the separations seen here are in agreement with previously reported results for SWNTs of similar diameters.[33]

On the basis of 20 micro-Raman spectra, we have calculated the diameters of 35 SWNTs using the Raman shifts of their radial breathing modes. Figure 8b shows that the diameters of the nanotubes measured this way are 1.4 ± 0.2 nm, within the distribution obtained from microscopy data. Notably, the diameter distribution measured from micro-Raman spectra is only a sampling of the true diameter distribution of the nanotubes, since resonant Raman experiments only detect nanotubes whose electronic energy spacings between van Hove singularities match the laser excitation energy (1.58 eV). Nevertheless, the spectroscopy data confirms the high quality of the synthesized SWNTs, and provides additional characterization of the structural parameters of SWNTs.

Conclusions

The main results presented in this article are summarized as follows. (1) We obtained discrete catalytic nanoparticles with tunable diameters by placing controllable amounts of iron (III) into the cores of apoferritin, followed by oxidation of the synthesized ferritin at high temperatures. Variations in the size of the catalytic nanoparticles were small, but still large relative to the mean diameter of the nanoparticles. There should be significant room for future work to refine the particle synthesis approach and narrow down the particle size distribution. (2) We have grown isolated single-walled carbon nanotubes from discrete catalytic nanoparticles by CVD, and the results demonstrate that the diameters of SWNTs can be controlled by tuning the size of catalytic nanoparticles. (3) We characterized our samples at single-particle and single-tube level by microscopy and spectroscopy techniques. We were able to image both ends of isolated CVD-grown SWNTs by TEM, and elucidate the microscopic relationship between catalytic nanoparticles and nanotubes. The growth mechanism for SWNTs in CVD is well described by the base-growth model. That is, the particle-containing growth-end of the nanotube remains anchored on the substrate, and the other end is dome-closed while extending out from the particle as the nanotube lengthens. During growth, the anchored nanoparticle only has a small surface area for carbon uptake from gas molecules, which makes the particle susceptible to poisoning effects and thus limits the length of the nanotube. Variations in particle size and local support-catalyst interactions/configurations are the likely causes to the different catalytic activities of nanoparticles in producing nanotubes. Further understanding of these factors will be important to controlling the lengths and eventually the chirality of SWNTs.

Acknowledgment. We thank Christopher Chidsey and Calvin Quate for discussions about general strategies to control the structures of nanotubes. This work was supported by NSF, the David and Lucille Packard Foundation, a Terman Fellowship, an ACS-PRF award and a Camille Henry Dreyfus New Faculty Award.

References and Notes

(1) Dresselhaus, M. S.; Dresselhaus, G.; Eklund, P. C. *Science of Fullerenes and Carbon Nanotubes*; Academic Press: San Diego, 1996.

(2) Dai, H. *Phys. World* **2000**, *13*, 43−47.

(3) Dai, H.; Kong, J.; Zhou, C.; Franklin, N.; Tombler, T.; Cassell, A.; Fan, S.; Chapline, M. *J. Phys. Chem. B* **1999**, *103*, 11 246−11 255.

(4) Kong, J.; Cassell, A. M.; Dai, H. *Chem. Phys. Lett.* **1998**, *292*, 567−574.

(5) Kong, J.; Soh, H.; Cassell, A.; Quate, C. F.; Dai, H. *Nature* **1998**, *395*, 878−881.

(6) Cassell, A.; Raymakers, J.; Kong, J.; Dai, H. *J. Phys. Chem. B* **1999**, *103*, 6484−6492.

(7) Cassell, A.; Franklin, N.; Tombler, T.; Chan, E.; Han, J.; Dai, H. *J. Am. Chem. Soc.* **1999**, *121*, 7975−7976.

(8) Franklin, N.; Dai, H. *Adv. Mater.* **2000**, *12*, 890−894.

(9) Hafner, J.; Bronikowski, M.; Azamian, B.; Nikolaev, P.; Colbert, D.; Smalley, R. *Chem. Phys. Lett.* **1998**, *296*, 195−202.

(10) Hafner, J.; Cheung, C.; Lieber, C. M. *J. Am. Chem Soc.* **1999**, *121*, 9750−9751.

(11) Su, M.; Zheng, B.; Liu, J. *Chem. Phys. Lett.* **2000**, *322*, 321−326.

(12) Dai, H.; Rinzler, A. G.; Thess, A.; Nikolaev, P.; Colbert, D. T.; Richard. E. Smalley *Chem. Phys. Lett.* **1996**, *260*, 471−475.

(13) Su, M.; Li, Y.; Maynor, B.; Buldum, A.; Lu, J. P.; Liu, J. *J. Phys. Chem. B* **2000**, *104 (28)*, 6505−6508.

(14) Li, Y.; Liu, J.; Wang, Y.; Wang, Z. L. *Chem. Mater.* **2001**, *13*, 1008−1014.

(15) Clegg, G. A.; Fitton, J. E.; Harrison, P. M.; Treffry, A. *Prog. Biophys. Mol. Bio.* **1980**, 36, 53−86.

(16) Meldrum, F. C.; Wade, V. J.; Nimmo, D. L.; Heywood, B. R.; Mann, S. *Nature* **1991**, *349*, 684−687.

(17) Wong, K. K. W.; Douglas, T.; Gider, S.; Awschalom, D.; Mann, S. *Chem. Mater.* **1998**, *10*, 279−285.

(18) Douglas, T.; Stark, V. T. *Inorg. Chem.* **2000**, *39*, 1828−1830.

(19) Yang, X.; Chen-Barrett, Y.; Arosio, P.; Chasteen, N. D. *Biochemistry* **1998**, *37*, 9743−9750.

(20) Yang, X. K.; Chasteen, N. D. *Biochem. J.* **1999**, *338*, 615−618.

(21) Kim, W.; Dai, H. unpublished result.

(22) Yang, P.; Zhao, D.; Margolese, D.; Chemelka, B.; Stucky, G. *Nature* **1998**, *396*, 152−155.

(23) Zhang, Y.; Franklin, N.; Chen, R.; Dai, H. *Chem. Phys. Lett.* **2000**, *331*, 35−41.

(24) Corio, P.; Brown, S. D. M.; Marucci, A.; Pimenta, M. A.; Kneipp, K.; Dresselhaus, G.; Dresselhaus, M. S. *Phys. Rev. B* **2000**, *61*, 13 202−13 211.

(25) Liu, J.; Dai, H. J.; Hafner, J. H.; Colbert, D. T.; Smalley, R. E.; Tans, S. J.; Dekker: C. *Nature* **1997**, *385*, 780−781.

(26) Martel, R.; Shea, H. R.; Avouris, P. *Nature* **1999**, *398*, 299.

(27) Tibbetts, G. G.; Devour, M. G.; Rodda, E. J. *Carbon* **1987**, *25*, 367−375.

(28) Tibbetts, G. G. *J Cryst. Growth* **1984**, *66*, 632−638.

(29) Baker, R. T. K. *Carbon* **1989**, *27*, 315−323.

(30) Amelinckx, S.; Bernaerts, D.; Zhang, X. B.; Van Tendeloo, G.; Van Landuyt, J. *Science* **1995**, *267*, 1334−1338.

(31) Dresselhaus, M. S.; Eklund, P. C. *Adv. Phys.* **2000**, *49*, 705−814.

(32) Jorio, A.; R Saito, R.; Hafner, J. H.; Lieber, C. M.; McClure, T.; Dresselhaus, G.; Dresselhaus, M. S. *Phys. Rev. Lett.* **2001**, *86*, 1118−1121.

(33) Kasuya, A.; Sugano, M.; Maeda, T.; Saito, Y.; Tohji, K.; Takahashi, M.; Sasaki, Y.; Fukushima, M.; Nighima, Y.; Horie, C. *Phys. Rev. B* **1998**, *573*, 4999−5001.